Title
SINTERING OF A12O3 POWDER COMPACTS I. DENSIFICATION KINETICS AND MICROSTRUCTURAL EVOLUTION

Author
Wang, D.N.K.

Publication Date
1977-05-01

Submitted to American Ceramic Society

LBL-6241
Preprint c.1

SINTERING OF Al_2O_3 POWDER COMPACTS I. DENSIFICATION KINETICS AND MICROSTRUCTURAL EVOLUTION

D. N. K. Wang and R. M. Fulrath

May 1977

Prepared for the U. S. Energy Research and Development Administration under Contract W-7405-ENG-48

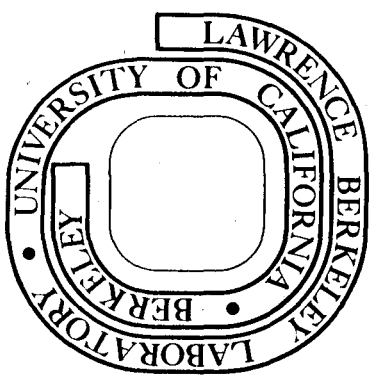

DISCLAIMER

SINTERING OF Al_2O_3 POWDER COMPACTS

I. DENSIFICATION KINETICS AND MICROSTRUCTURAL EVOLUTION

D. N. K. Wang and R. M. Fulrath

Materials and Molecular Research Division, Lawrence Berkeley Laboratory
and Department of Materials Science and Mineral Engineering,
University of California, Berkeley, California 94720

ABSTRACT

A constant heating rate technique was utilized to study MgO-doped Al_2O_3 powder compacts with variations in green density. Hot stage scanning electron microscopy was used to monitor continuously the linear dimensional change of a powder compact throughout the densification process at various constant heating rates. The maximum densification rate was found to occur at a critical density which was independent of the heating rate as long as the green density remained constant. Microstructural evolution has been correlated with the densification rate to explain the occurrence of the maximum rate of densification. It was found that the densification rate, after the achievement of the critical density, is strongly dependent on porosity.

INTRODUCTION

During the past 30 years, a large number of studies have been made in an attempt to provide a better general understanding of the sintering process. Aluminum oxide has been one of the most widely used materials for these investigations. The influence of surface energy as the driving force for sintering, the importance of diffusion process for mass transport[1], and the role of grain boundaries as vacancy sinks[2] seem well established for the polycrystalline solid state system. Despite extensive research activity concerning the theory of sintering, there has been little translation of theory to practical application. Mechanistic studies have relied heavily on simple models. However, in a real powder system, particles rarely have regular forms, and they are never simply distributed. In addition, there are fluctuations in density originating from powder agglomeration and uneven compaction. At this point in time, it seems unlikely that a precise prediction of a density-time-temperature relationship can be achieved for the whole course of the sintering process. Therefore, a thorough phenomenological study of the densification kinetics and the microstructural evolution kinetics, as well as correlations of these kinetics from the start to the completion of the sintering process, is important.

Previous sintering studies[3,4] have concentrated on the use of isothermal techniques. A complete analysis of sintering kinetics is unattainable due to uncertainties involved in the initial heating period. The type of heating program that can be treated analytically and which approaches practical application is a constant rate of heating. This work has used a constant heating rate technique to obtain a detailed analysis of the kinetics of sintering aluminum oxide powder compacts.

EXPERIMENTAL PROCEDURE

Two different types of aluminum oxide powders were used in this study. Most of the work involved the use of autoclaved high purity aluminum oxide which was received in the form of plates with a diameter of 2 inches and a thickness of 0.125 inch from the General Electric Company. Compacts were made by cold pressing submicron aluminum oxide particles (0.2μm), to which 0.1 wt% of MgO and 8 wt% of an organic binder were added. These compacts were prefired at 650°C in air for one hour to decompose the organic binder. After this treatment, the outer and central portions of the compacts were discarded, and the rest of it was broken into pieces approximately one centimeter square. Specimens used for the sintering experiments were then cut and shaped from these pieces. This method of specimen preparation minimized the variations in the green density caused by any pressure gradients during powder compaction. All the specimens had a diameter of 0.2 inch and a thickness of 0.125 inch with the same green density of 40% of theoretical. The green density was determined for each piece by mercury displacement.

Union Carbide Linde-A Al_2O_3 powder (0.3μm) was used to study the effect of green density on the sintering behavior. This powder was mixed with isopropyl alcohol and appropriate amounts of a polyvinyl alcohol-saturated water solution and magnesium nitrate in order to yield 8 wt% of organic binder and 0.1 wt% of MgO in the Al_2O_3 powder, respectively. After mixing, the slurry was dried, screened through a 44μm sieve, and cold pressed in a steel die. To obtain variations in green densities, the powder was compacted at various pressures, but the bulk specimen volume was kept constant by adjusting the amount of powder used.

All the pressed specimens had approximately a 0.2 inch diameter and a 0.1 inch thickness. The green densities of the specimens were determined after prefiring at 650°C in air for one hour.

Compacts of different green densities were heated at various rates in the hot stage scanning electron microscope. In each run, the specimen was first heated to 800°C, and then the temperature was increased to 1700°C or higher at a controlled rate. The fractional shrinkage was determined using a marker technique[5], and the density was calculated by using the equation

$$\rho = \frac{\sum_{i}^{n} \rho_o / (1 - \frac{\Delta L}{L_o})_i^3}{n} \qquad (1)$$

where ρ = average density at any time or temperature,

ρ_o = green density of the specimen,

$\frac{\Delta L}{L_o}$ = fractional shrinkage in each measurement after thermal expansion correction at any temperature, and

n = number of measurements at any temperature.

The relative density value was obtained by dividing this calculated value by the theoretical density, 3.98 g/cm^3.

Compacts used for the microstructure study were heated in the hot stage at programmed heating cycles to desired densities and cooled by quenching. A sulfur impregnation technique was used for all low density samples ($\lesssim$95% theoretical) to preserve the microstructure during polishing. After being polished, the impregnated sulfur was sublimed, and the samples were thermally etched in air at temperatures from 1100°C to 1250°C for various periods of time up to two hours depending on the sample density. Temperature and time were selected to avoid any

additional microstructural changes induced by excessive firing during the etching process.

High magnification pictures, from 10,000X to 20,000X, were taken for a quantitative study of grain growth. Since high magnification pictures cover too small an area to obtain an average quantitative value, several pictures were taken in different areas of each sample. In order to determine an average grain size for porous samples, photographs were placed underneath a transparent plastic sheet, on which parallel lines had been drawn. Segments of lines, formed by the interceptions of grain edges with those parallel lines, were measured individually, and 500 to 800 of those segments were averaged to yield a preliminary value. This value was then corrected for magnification factors and multiplied by 1.5 to give an average grain size.[6]

RESULTS AND DISCUSSION

A. Description of the Green State

Particles formed from a salt solution may agglomerate at some point during the decomposition - calcination process.[7] If agglomeration does not occur during powder formation, pre-compaction granulation may cause agglomeration of particles. Granulation is an essential step for increasing the pressed density and improving the homogeneity of the compact by improving the inherently poor flow properties of fine particles. Since voids contained in a green compact are determined by the packing of particles, the presence of agglomerates will make the pore size, location, and distribution more complex than assumed in models. A profound influence would be expected on both the rate of sintering and, more inportantly, the residual porosity.

Scanning electron fractographs of a prefired green compact at different magnifications are shown in Fig. 1. This type of compact, having an initial density of 40% of theoretical, was used for most of the present work. As seen in Fig. 1A, agglomerates of about 30μm diameter resulted from the granulation operation. The details of particle packing can be seen in higher magnification photographs, Figs. 1B and C. In addition to the large agglomerates (granules), Fig. 1C shows that there are numerous small agglomerates formed by several individual particles. These clusters of particles are generally closely packed and contain very fine pores of nearly uniform size. However, the inter-cluster pores are not uniformly distributed in size, shape, and location. In the present work, quantitative measurement of pore size distribution was not made. However, from the photographs, one can see that the pore

size distribution in the compact is probably trimodal. This is further illustrated in Fig. 2 where pressed compact surfaces are shown for two different types of Al_2O_3 powders.

As previously illustrated in Fig. 1, void volume between agglomerates is larger than those within and between clusters. As sintering proceeds, these void volumes develop into pores. The pores originating in and between the clusters are small, while those originating between agglomerates are large. The flux of lattice vacancies away from the small pores will be larger than that from the large pores, while the volume of material needed to fill the larger pore is greater. For these reasons, large pores will remain much longer than small ones in a sintered body.

Ceramographic examination clearly points to this occurrence. The first picture in Fig. 3 shows a fracture surface of a green compact. The next two are the polished surfaces of the compacts sintered to 85% and 90% of theoretical density, respectively. The middle microstructure reveals that within individual agglomerates sintering occurs quickly, while a network of coarse porosity between them persists. The third picture shows the two dimensional inter-agglomerate boundary. This illustrates that the pores in the corners of agglomerates as well as the pores in the agglomerate boundaries will persist if early cohesion is not achieved during sintering. This residual porosity is not generally related to particle size, but rather to the type of powder and powder processing. As a result, the term "powder sinterability" should not be determined by referring only to surface area per unit volume of the powder, but must also take into account the particle packing which

affects pore size, shape and distribution.

In addition to the presence of agglomerates, density inhomogeneity is also important when discussing the effect of green state on the sintering kinetics. The density variation caused by die wall friction during compaction will be referred to as macro-inhomogeneity, since it will cause anisotropic shrinkage of the compact on a large scale. The type of inhomogeneity caused by the particle agglomeration will be referred to as micro-inhomogeneity. The presence of agglomerates causes local variations in pore size and distribution, but in the absence of uneven compaction, these variations will be the same everywhere throughout the compact, and the sample will not show an anisotropic shrinkage during sintering. Since the hot stage scanning electron microscopy allows the study of linear shrinkage of a compact in two dimensions, this technique is able to demonstrate the effect of macroscopic homogeneity and inhomogeneity upon the linear dimensional change of a powder compact during sintering. A comparison was made by selecting one specimen near the edge and another near the center of a two inch diameter cold pressed plate. The one near the edge (W-7) is considered to be macroscopically inhomogeneous, since it was subjected to die wall friction. The one near the center (W-5) is considered to be macroscopically homogeneous, since it was subjected to a uniform compaction pressure. Results of these two sintering runs, in which the samples were heated at a rate of 4°C/min to temperatures of 1350°C (W-5) and 1385°C (W-7), are shown in Fig. 4. After reaching the individual temperatures, the samples were held isothermally. In both curves, every datum point is the average of nine individual shrinkage measurements. Sample W-5 showed

isotropic shrinkage with little scatter in the data. The statistical scatter in the measurements for W-7 indicated that this sample shrank inhomogeneously. This is illustrated dramatically by overlaying a magnified picture of the final marker positions on the picture of the original positions. Although the two samples behaved differently in sintering, their mean average values of nine measurements at each point coincide very well.

B. Densification Kinetics

Figure 5 gives the change of relative density with temperature for four different heating rates using compacts with a green density of 40% of theoretical. Two runs were made for each heating rate in order to generate more accurate experimental results. As indicated by the curves, the slower the heating rate used, the higher the density at any given temperature. By measuring the tangent of the curve at a given temperature and by utilizing the equation dT - adt, the densification rate, dρ/dt, can be determined for any particular temperature. The results are presented in Figs. 6 and 7. Figure 6 shows that the densification rate increases with temperature to a maximum value and then decreases. Examination of densification rate versus relative density curves in Fig. 7 reveals that the maximum value occurs at the same relative density, about 0.73, which is independent of heating rate and temperature. The difference in the values of the maximum densification rate for different heating rates is attributed to the difference in temperatures at which the maximum rate occurs, as illustrated in Fig. 7. The occurrence of a maximum densification rate indicates that there must be microstructural changes during the densification process which are vital to the densification behavior.

These changes can be generally divided into three categories: (1) evolution of grain structure (2) evolution of a pore phase, and (3) the change of the pore-grain boundary geometry. At this point, it is assumed that the major cause for the occurrence of a maximum densification rate at a constant relative density, independent of the heating rate used, is the distinct change of the pore phase. Therefore, it is expected that the maximum densification rate will shift to a different value of relative density as the green density varies. A variation in green density will cause a change of particle packing, and, therefore, will change pore size and pore distribution in the powder compact. Figure 8 shows that the occurrence of the maximum densification rate shifts toward a lower relative density value as the green density of the compact decreases. Because small pores disappear first, the smaller number of small pores in a low green density compact will, therefore, lead to a lower density before the densification rate starts to decrease.

Further evidence of the effect of the evolution of pore phase on the densification rate can be obtained by examining the development of microstructure of compacts during sintering. Figure 9 consists of six microphotographs which were taken from polished surfaces of fired compacts. The number appearing on the upper left hand corner of each photograph represents the value of relative density. It is apparent that the average pore size increases and the number of pores decreases as density increases. As sintering proceeds, the pore size distribution will gradually shift to a larger average pore size through the elimination or reduction in size of the small pores.

Kingery and Francois[8] working with UO_2, observed an increase in pore diameter when the material was annealed long enough at high temperature. They proposed that pore growth results from coalescence due to pore migration which accompanies grain growth. Kuczynski[9] argued that pore growth was caused by a volume diffusion process (Ostward ripening) by which large pores grow at the expense of small pores. However, by examining the shape and geometry of the large pores in the final microstructure (P=0.97) in Fig. 9 and by tracing their history back to the low density microstructures, it appears that these large pores result directly from the inter- agglomerate pores in the green compact rather than as a result of pore growth.

Figure 9 illustrates a transition region between 70% and 80% relative density in terms of the uniformity of the distribution of inter-particle and inter-cluster pores (the inter-agglomerate pores are excluded from this observation, since the high magnification used for these photographs allows coverage of only a few agglomerates). Microstructures developed at, or below, the relative density of 70% have a fairly uniform distribution of pores, since densification to this point is due mainly to reduction in size and elimination of inter-particle pores and reduction in size of inter-cluster pores. Microstructures developed at, or above, the relative density of 80% do not have a uniform distribution of pores. In this stage of sintering, densification results mainly from a reduction in size of inter-cluster and inter-agglomerate pores as well as the elimination of some inter-cluster pores. As described earlier, there is a size distribution for inter-cluster pores, and, therefore, after the elimination of small inter-cluster pores, large inter-cluster pores are

left resulting in a non-uniform porosity distribution. The non-uniform distribution of pores, i.e., the local variation in pore concentration, is usually more important than the range of pore size as far as the rate of densification is concerned. It is supposed that this local variation in pore concentration and the increase in average pore size are the reasons that the densification rate becomes highly density dependent. The occurrence of the maximum densification rate at a relative density of 73% (Fig. 7) coincides with the occurrence of a transition state (between relative densities of 70% and 80% in Fig. 9) that depends on the pore concentration and size distribution.

In addition to the evolution of pores, the evolution of grain structure and pore-grain boundary geometry are also important to densification kinetics. Scanning electron microphotographs taken from polished, and subsequently etched, surfaces of compacts which were heated at the same rate of 4.6°C/min from a 40% green density to different densities are shown in Fig. 10. In order to obtain more representative pictures, only areas inside agglomerates were selected, and, therefore, the pores shown in these pictures include only inter-particle and inter-cluster pores. Several features should be noted: (1) the grain (particle) size increases as density increases, and considerable grain growth has occurred even at the very early stage of sintering, (2) all the pores either intersect grain boundaries or are located in four grain corners, depending on the initial particle packing,(3) the shape of the grains (particles) change as sintering proceeds; initially, the particles appear to be chain-like (Figs. 10B and C), then to be oblong (Fig. 10D), and finally, to be equiaxed

(Figs. 10E, F, G and H), and (4) the local variation in pore concentration allows the growth particles in the dense regions and results in a broader grain size distribution as compared with that in the low density microstructures. In accordance with the changes of particle shape and pore concentration as shown in Fig. 10, a transition regions occurs between relative densities of 70% to 75% which again agrees quite well with the density found for the occurrence of the maximum densification rate.

A study of the heating rate effect on microstructural evolution is required before any further quantitative analysis of the densification kinetics is possible. A plot of grain size vs. density for compacts with green density of 40% of theoretical and doped with 0.1 wt% MgO is shown in Fig. 11. The grain size remains the same for a given density irrespective of the heating rate. This relation indicates that, for this range of heating rates (2.5°C to 9.4°C/min), the evolution of microstructure is insensitive to heating rate as long as the green density remains the same. Figure 12 gives the results which were generated from Linde-A Al_2O_3 compacts of three different green densities sintered at the same heating rate (4.6°C/min). Previous measurements by Lay and Greskovich[10] using an isothermal sintering technique are also plotted in Fig. 12 to compare with the present results. Agreement is good until the curves start to bend upward. This agreement further shows the grain size - density relationship is independent of heating rate and temperature, as long as the green density of the compact is kept constant. Figures 11 and 12 also illustrate that the grain size and density are linearly related until a particular density is reached.

The density at which the linearity ends varies with green density. The densities at the bending points are approximately 75% of theoretical for the curve shown in Fig. 11 and 65%, 75% and 78% for green densities of 32%, 38% and 48% of theoretical, respectively, in Fig. 12. These values are about the same values that have been observed in Figs. 7 and 8 as the densities at which the maximum densification rate occurs. After the critical density is reached, local variation in pore concentration is developed, and, consequently, grain growth in denser regions is no longer retarded by the presence of pores. This is the reason for the upward curve in the relationship between grain size and relative density after the critical density is reached.

At a given density, the microstructural features (such as grain size, pore size, pore shape, and pore-grain boundary geometry) are assumed (based on the quantitative and quantitative evidence presented) to be fixed during the sintering process, independent of heating rate used. The rate of the densification process can then be described by the following empirical equation regardless of the detailed mechanisms and the microstructural evolution with change of density.

$$\frac{d\rho}{dt} = \frac{K\exp(-\frac{Q}{RT})}{kT} P^n \qquad (2)$$

where $\frac{dP}{dt}$ and P are densification rate and fractional porosity ($P = 1-\rho$) at any temperature, respectively. Q is the apparent activation energy for the densification process, n and K are constants, R is the gas constant, k is the Boltzmann constant, and T is the sintering temperature (°K) at which $\frac{d\rho}{dt}$ and P are determined. Therefore, a plot of $\ell n\ T\frac{d\rho}{dt}$ vs. $\frac{1}{T}$ with relative density, ρ, kept constant should give a straight line,

if the apparent activation energy does not change during the densification process. In Fig. 13 four values of $\ell nT\frac{d\rho}{dt}$ (one for each heating rate) at four temperatures are plotted from a relative density of 50% to 98%.

The apparent activation energy calculated from the slopes gives two values. For densities below 55% of theoretical, the activation energy is approximately 90 Kcal/mole, while for densities above 55%, the activation energy is approximately 150 Kcal/mole. The low value of 90 Kcal/mole is about the same value (93 Kcal/mole) determined for the initial stage sintering by the present authors on the same material.[5] The high value of 150 Kcal/mole determined in the present work agrees very well with the values of 153 Kcal/mole and 150 Kcal/mole reported by Coble[3] and Bruch[4], respectively. The deviation of points with high heating rates at densities of 95.5% and 97% is attributed to the larger average grain size as compared to those obtained at lower heating rates.

The observation of a single-valued apparent activation energy for the whole densification process, except for the initial stage, suggests that a single diffusion mechanism or a combination of mechanisms with the same activation energy predominates over the entire temperature range.

By assuming a volume diffusion mechanism and by assuming the interior geometry of the compact to be represented by a system of uniform cylindrical pores situated on all the edges of polyhedra of uniform size, Coble[11] derived an equation to predict the time-dependence for intermediate stage sintering. Based on his assumptions, the equation is correct, if it is presented in the form of

$$\frac{d\rho}{dt} = \frac{ND_v\gamma\Omega}{\ell^3 kT} \tag{3}$$

where $\frac{d\rho}{dt}$ is the densification rate at absolute temperature T, N is a numerical factor[12] having the value of 335, D_v is the volume diffusion coefficient, γ is the surface energy, Ω is the volume of a vacancy, ℓ is the edge length of the grain, and k is the Boltzmann constant. Since $D_v = D_o \exp(-\frac{Q}{RT})$ and $\ell \simeq G$, the equation becomes, after rearrangement,

$$\frac{\frac{d\rho}{dt} G^3 T}{\exp(-\frac{Q}{RT})} = \frac{ND_o\gamma\Omega}{k} = \text{constant} \tag{4}$$

In order to check the applicability of Coble's equation to the present results, simultaneous measurements of densification rate and grain size at their corresponding temperature were made. Using the value of 150 Kcal/mole as the apparent activation energy, Q, the values for the left hand side of equation (4) were calculated and plotted against porosity in Fig. 14. As shown in Fig. 14, Coble's equation for sintering kinetics holds up to a density of 70% of theoretical (30% porosity). The linear relationship between porosities of 30% and 5% can be explained by the interdependence of densification and grain growth kinetics which will be discussed in Part II. Because the occurrence of the breaking point (70% relative density in Fig. 14) agrees well with the critical density value observed in Fig. 7, the inapplicability of Coble's equation can, therefore, be explained in terms of the local variation in pore concentration. The reduction in the total number of pores and the increase of the average pore size after the critical

density is achieved were not taken into account in Coble's equation.

The values of the diffusion coefficients, D_v, for compacts of different green densities and powders are calculated from their sintering kinetics before the achievement of their corresponding critical densities using equation (3) (with γ = 1,000 erg/cm^2 and $\Omega = 1.4 \times 10^{-23}$ cm^3). These values are shown in Fig. 15 along with Coble's result. The activation energy calculated from these results is the same value, 150 Kcal/mole, determined in Fig. 13 for shrinkage of pores only.

The reason for the discrepancy observed in diffusion coefficients for different green density compacts may be attributed to the difference in their microstructures. The ratio (number of grains between small pores to pore spacing) is assumed to be higher for low green density compacts than for high green density compacts, because a higher total number of small pores are present in the high green density compact. If the densification for this stage results from shrinkage of small pores, then the ratio of effective diffusion path length to the grain size is higher for low green density compact than for high green density compact. Therefore, this will change the calculated diffusion coefficient, if G is considered to be the grain size instead of the effective diffusion path length.

CONCLUSIONS

The particle packing and the resultant porosity distribution in a green compact has a very important effect on microstructural development and sintering kinetics. The term "powder sinterability" should, therefore, not only be determined by referring to the surface area per unit volume of the powder, but also must take into account the particle packing which affects pore size, shape, and distribution.

The maximum densification rate was found to occur at an initial density which was independent of the heating rate as long as the green density remained constant. This critical density shifts toward a lower value as the green density of the compact decreases.

The activation energy for the shrinkage of pores was determined to be 150 Kcal/mole which agrees well with previous reports on the same material. Simultaneous measurements of densification rate and grain size have shown that Coble's sintering equation is not applicable after the critical density is reached. The porosity dependence of the densification rate after the achievement of the critical density has been attributed to the decrease in total number of pores and the increase in average pore size as densification proceeds.

ACKNOWLEDGEMENT

This work was supported under the auspices of the United States Energy Research and Development Administration.

REFERENCES

1. G. C. Kuczynaki, "Self-Diffusion in Sintering Metal Powders," Trans. Amer. Inst. Min. (Metall.) Engrs., 185, 169 (1949).

2. B. H. Alexander and R. W. Balluffi, "Mechanism of Sintering of Copper," Acta Met. 5[11] 666-77 (1957).

3. R. L. Coble, "Sintering Crystalline Solids: II. Experimental Test of Diffusion Models in Powder Compacts," J. Appl. Phys., 32 [5] 793-799 (1961).

4. C. A. Bruch, "Sintering Kinetics for the High Density Alumina Process," Bull. Am. Ceram. Soc., 41 [12] 799-806 (1962).

5. D. N. Wang, and R. M. Fulrath, "Initial Sintering of Al_2O_3 Powder Compacts by Hot Stage Scanning Electron Microscopy," submitted to the Journal of the American Ceramic Society.

6. R. L. Fullman, "Measurement of Particle Sizes in Opaque Bodies," Trans. AIME, 197 [3] 447-452 (1953).

7. D. W. Johnson, D. J. Nitti and L. Berrin, "High Purity Reactive Alumina Powders: II. Particle Size and Agglomeration Study," Bull. Am. Ceram. Soc., 51 [12] 896-900 (1972).

8. W. D. Kingery and B. Francois, "Grain Growth in Porous Compacts," J. Amer. Ceram. Soc., 48 [10] 546-547 (1965).

9. G. C. Kuczynski, "Pore Shrinkage and Ostward Ripening," in "Sintering and Related Phenomena," Materials Sci. Res. [6], 217, Plenum Press, NY (1973).

10. C. Greskovich and K. W. Lay, "Grain Growth in Very Porous Al_2O_3 Compacts," J. Amer. Ceram. Soc., 55 [3] 142-146 (1972).

11. R. L. Coble, "Sintering Crystalline Solids, I. Intermediate and Final Stage Diffusion Models," J. Appl. Phys., 32 [5] 787-792 (1961).

12. R. L. Coble and T. K. Gupta, "Intermediate Stage Sintering," in "Sintering and Related Phenomena," G. C. Kuczynski, N. A. Hooton, and C. F. Gibbon eds., Gordon and Breach, NY, 423-443 (1967).

FIGURE CAPTIONS

1. Scanning electron fractograph of prefired G. E. Al_2O_3 powder compact with a green density of 40% of theoretical taken at three different magnifications.
2. Scanning electron micrographs taken from pressed compact surfaces (A and C, G. E. powder; B and D, Union Carbide powder).
3. Evolution of inter-agglomerate porosity at different degrees of sintering for G. E. Al_2O_3 powder compact. Top to bottom: Green compact (40%), 85%, and 90% relative density.
4. Effect of macroscopic green density inhomogeneity on sintering behavior.
5. The relative density of 0.1 wt% MgO-doped G. E. Al_2O_3 powder compact as a function of temperature for four constant heating rates.
6. The densification rate of MgO-doped G. E. Al_2O_3 powder compacts as a function of temperature.
7. The densification rate of MgO-doped G. E. Al_2O_3 powder compacts as a function of relative density.
8. Densification rate vs. relative density for MgO-doped Al_2O_3 powder compacts with various green densities heated at a constant rate of 4.6°C/min.
9. Evolution of the pore phase of MgO-doped G. E. Al_2O_3 (40% green density) powder compacts sintered at a rate of 4.6°C/min. The number appearing on the upper left hand corner of each photograph represents the value of relative density.

10. Evolution of the microstructure of MgO-doped G. E. Al_2O_3 (40% green density) sintered at a constant rate of 4.6°C/min. The number appearing on the upper left hand corner of each photograph represents the value of relative density.
11. Grain size vs. relative density for 0.1 wt% MgO-doped G. E. Al_2O_3 powder compacts (40% green density) heated at three rates.
12. Grain size vs. relative density for 0.1 wt% MgO-doped and undoped Union Carbide Al_2O_3 powder compacts with different green densities heated at a rate of 4.6°C/min. Isothermal data (Ref. 23) is presented for comparison.
13. $\ln T\,(d\rho/dt$ vs. $\frac{1}{T}$ for 0.1 wt% MgO-doped G. E. Al_2O_3 powder compacts with a 40% green density heated at four rates.
14. $(d\rho/dt)G\,T/\exp(-\frac{G}{RT}$ vs. porosity, P, plot using Coble's intermediate stage sintering equation (Ref. 12) for MgO-doped G. E. Al_2O_3 powder compacts.
15. Diffusion coefficients calculated from sintering data, using Coble's equation, with Coble's sintering result.

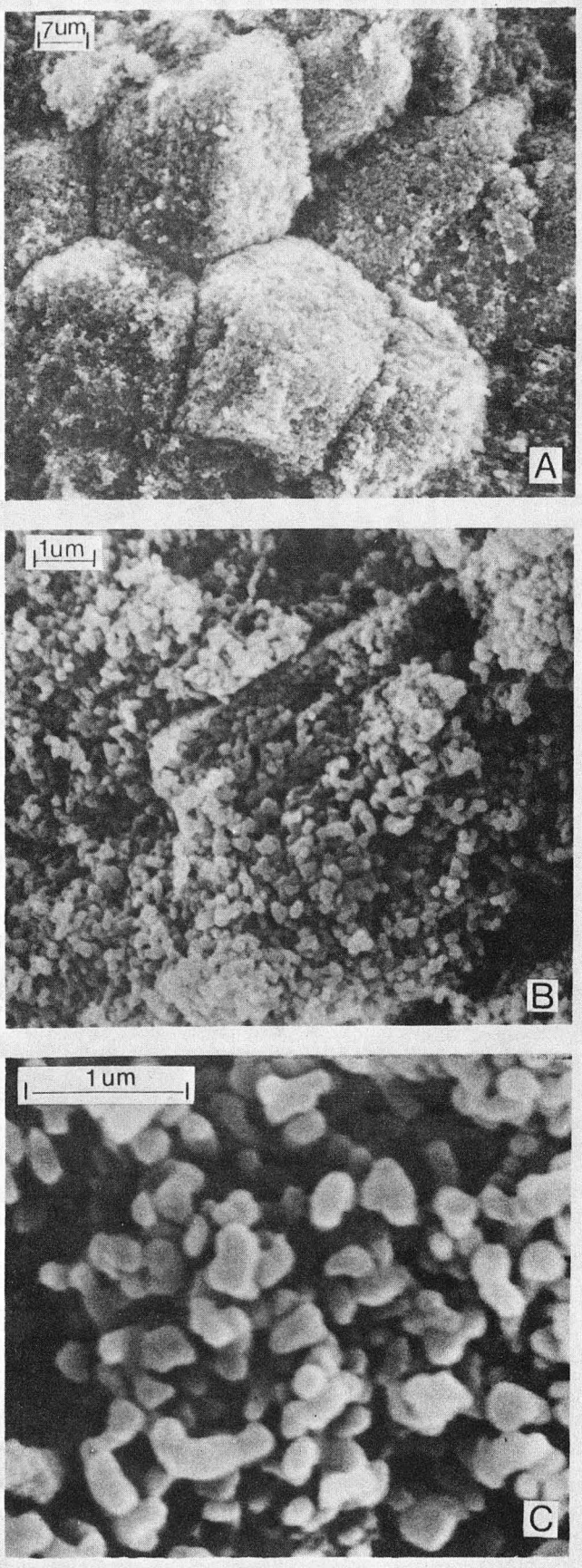

XBB7610-7852

Figure 1.

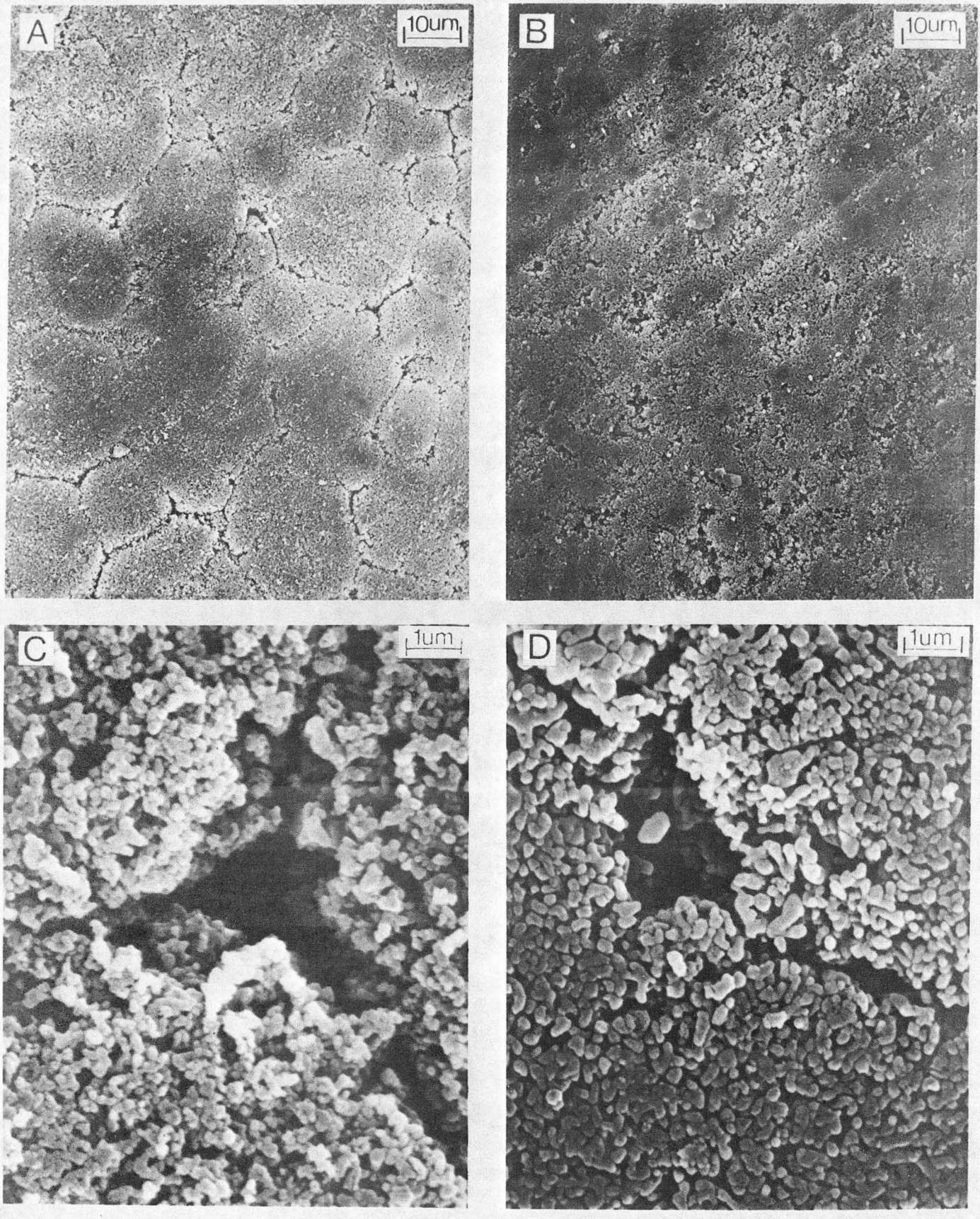

XBB768-7110

Figure 2.

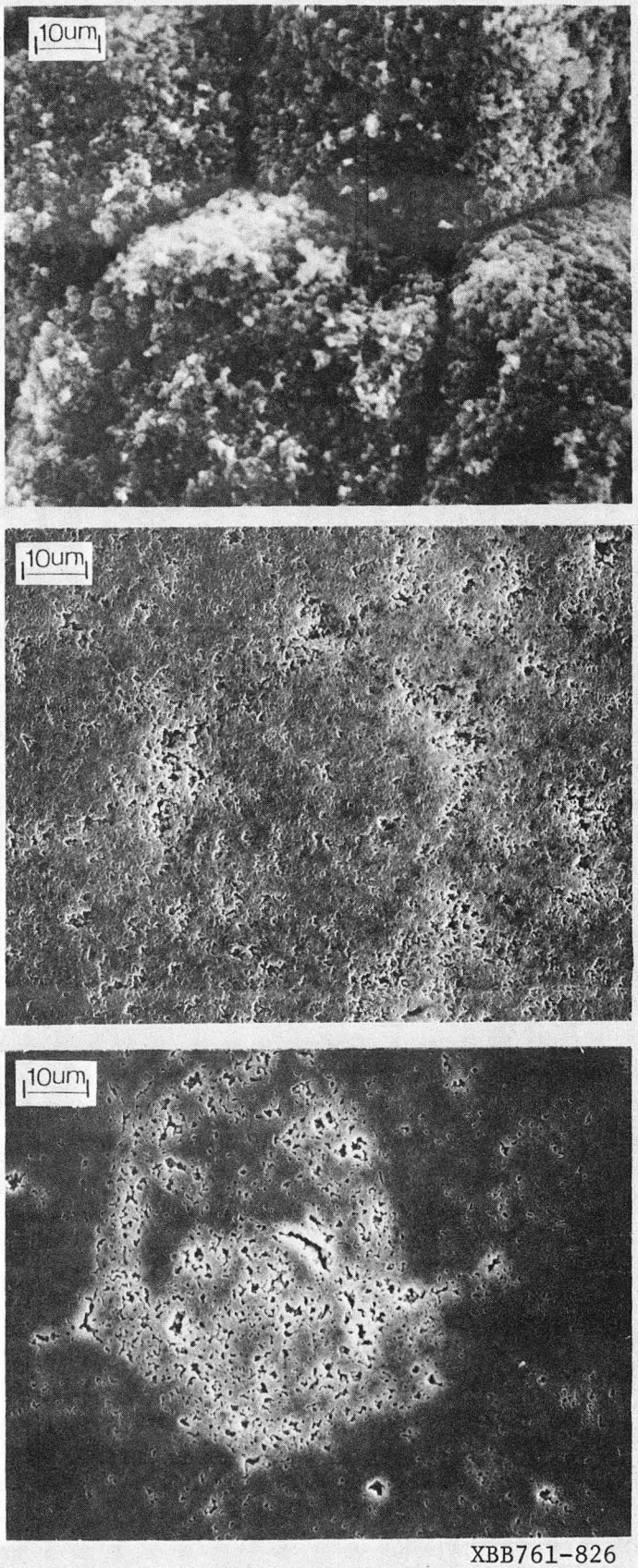

XBB761-826

Figure 3.

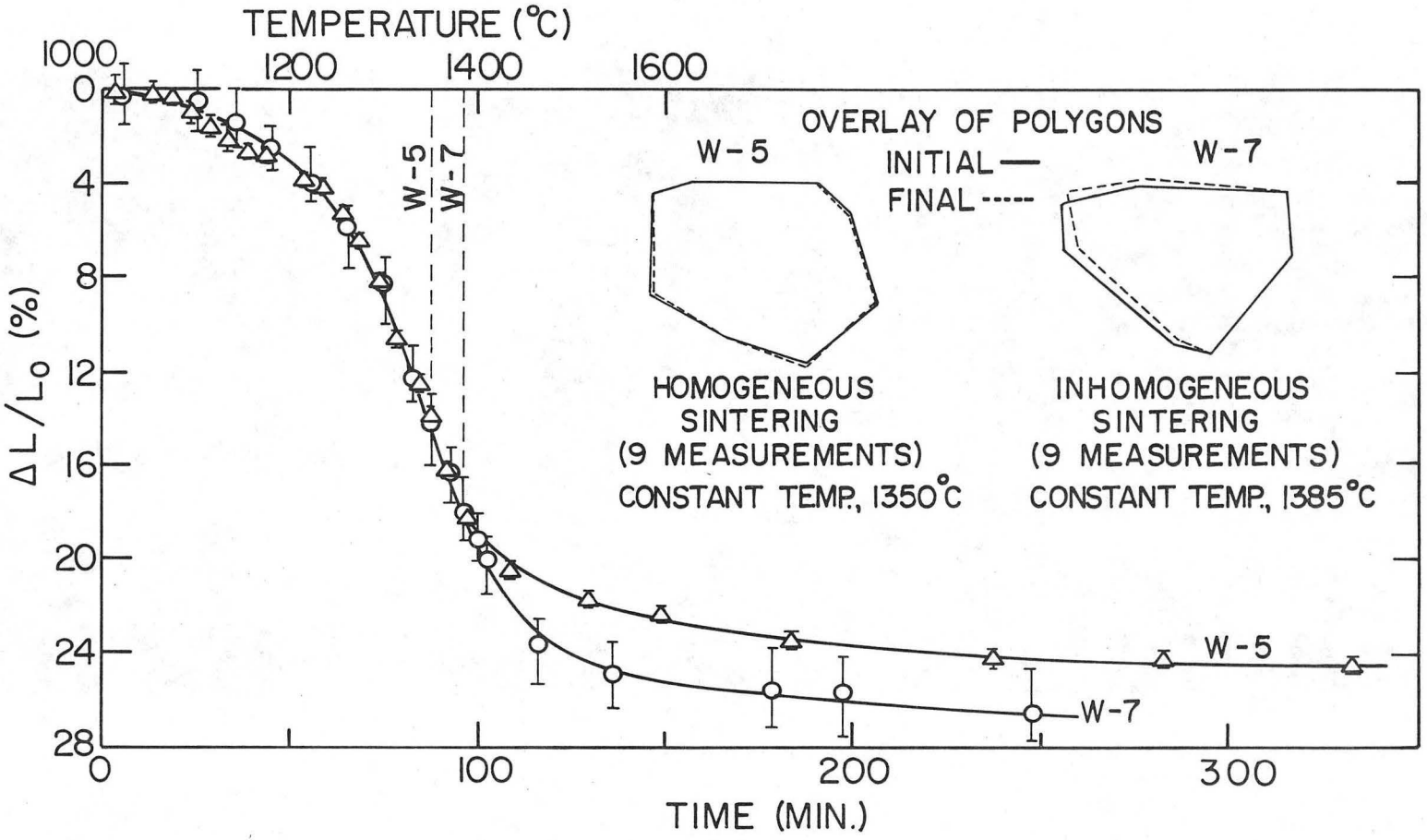

XBL742-5585

Figure 4.

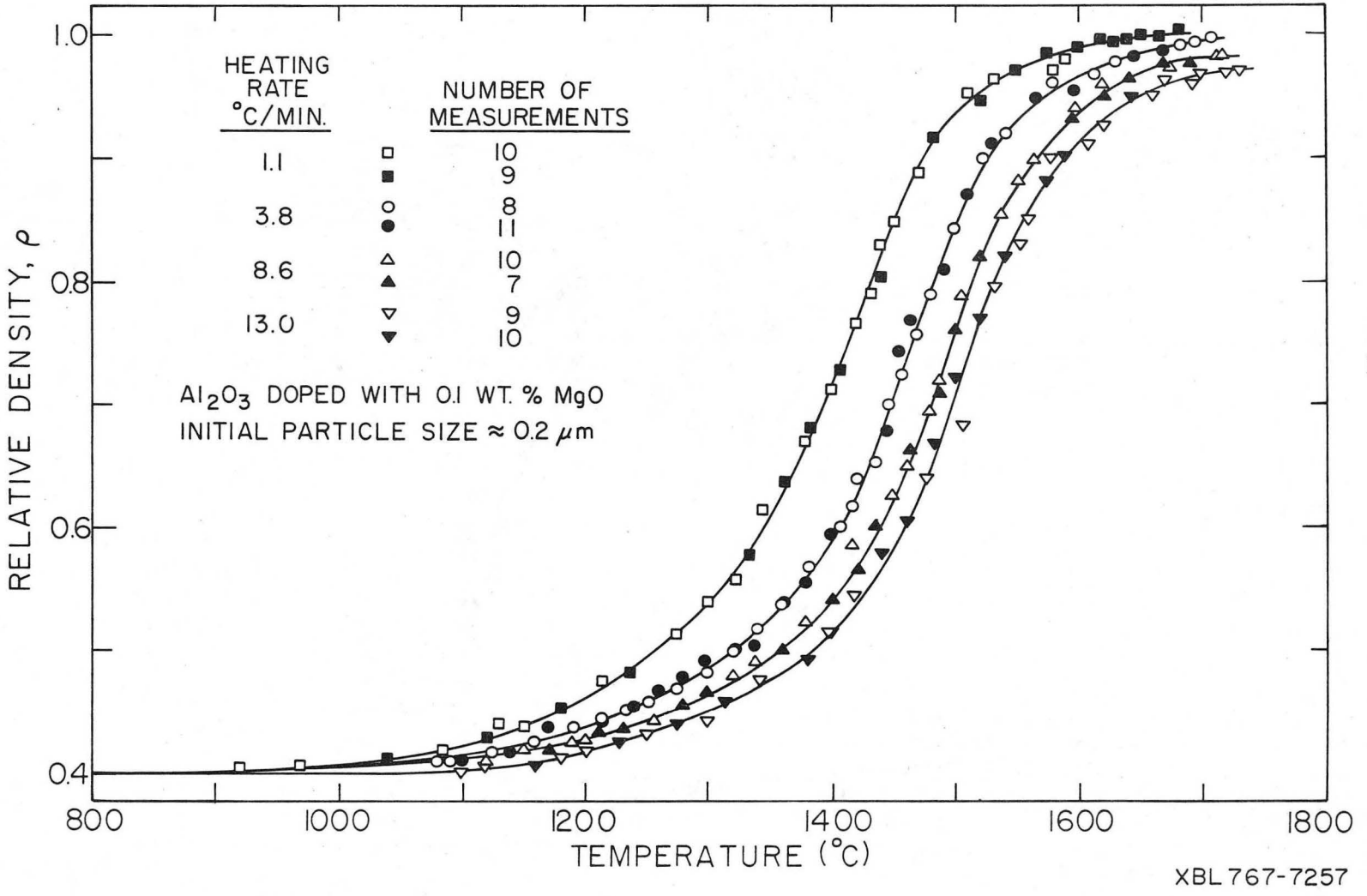

Figure 5.

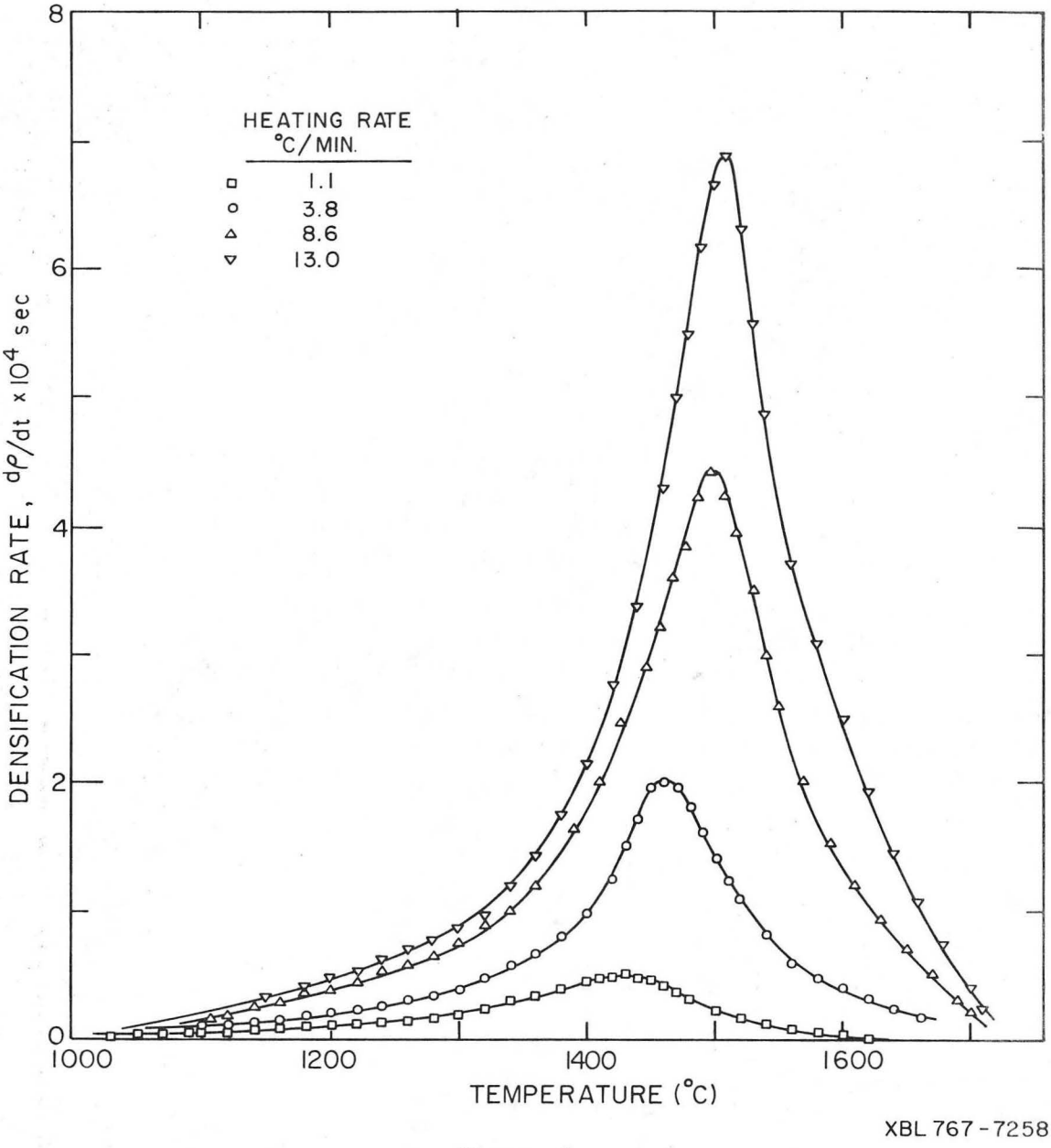
HEATING RATE
°C/MIN.
1.1
3.8
8.6
13.0
DENSIFICATION RATE, dρ/dt x 10⁴ sec
TEMPERATURE (°C)
0
2
4
6
8
1000
1200
1400
1600
XBL 767-7258

Figure 6.

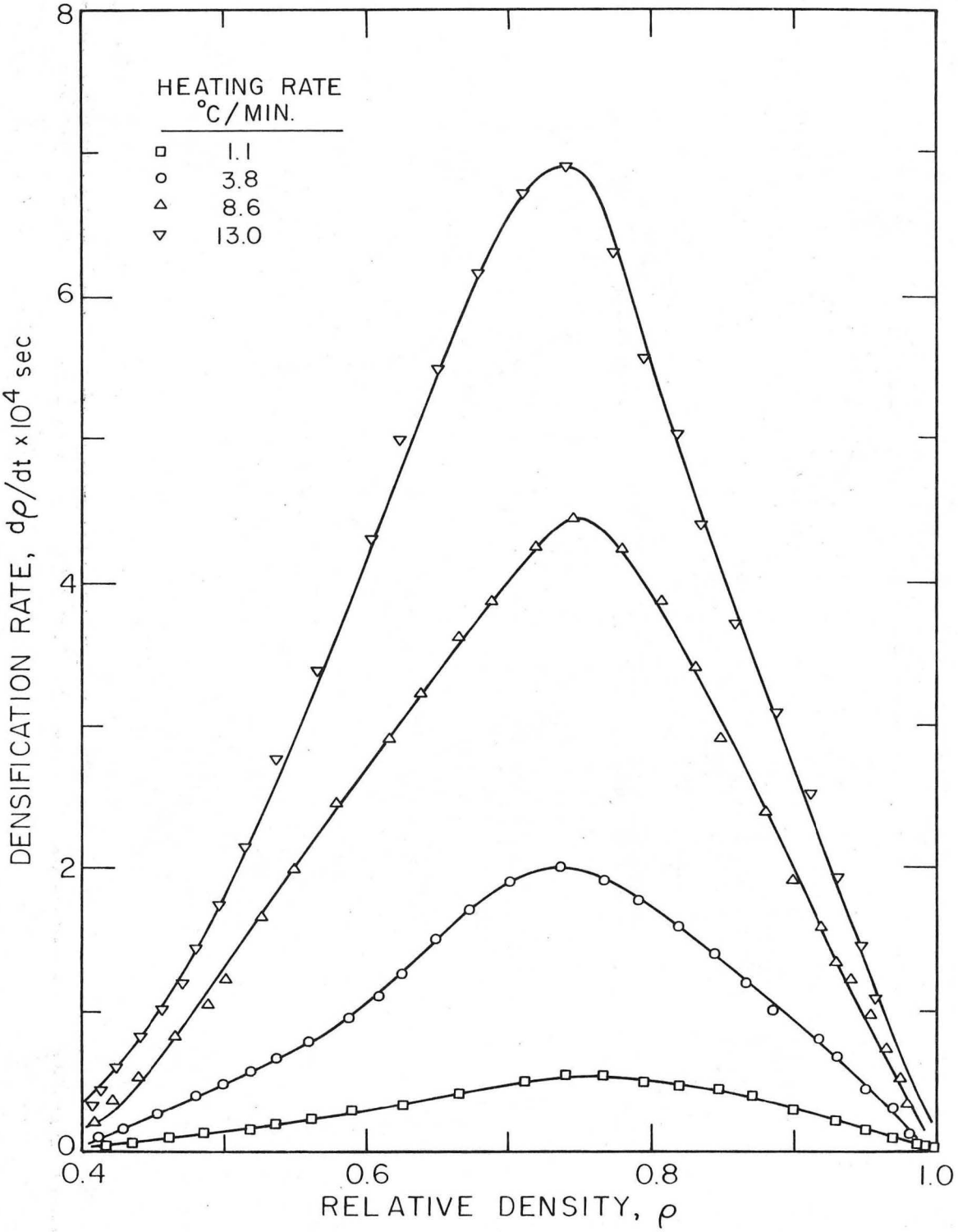

XBL 767-7259

Figure 7.

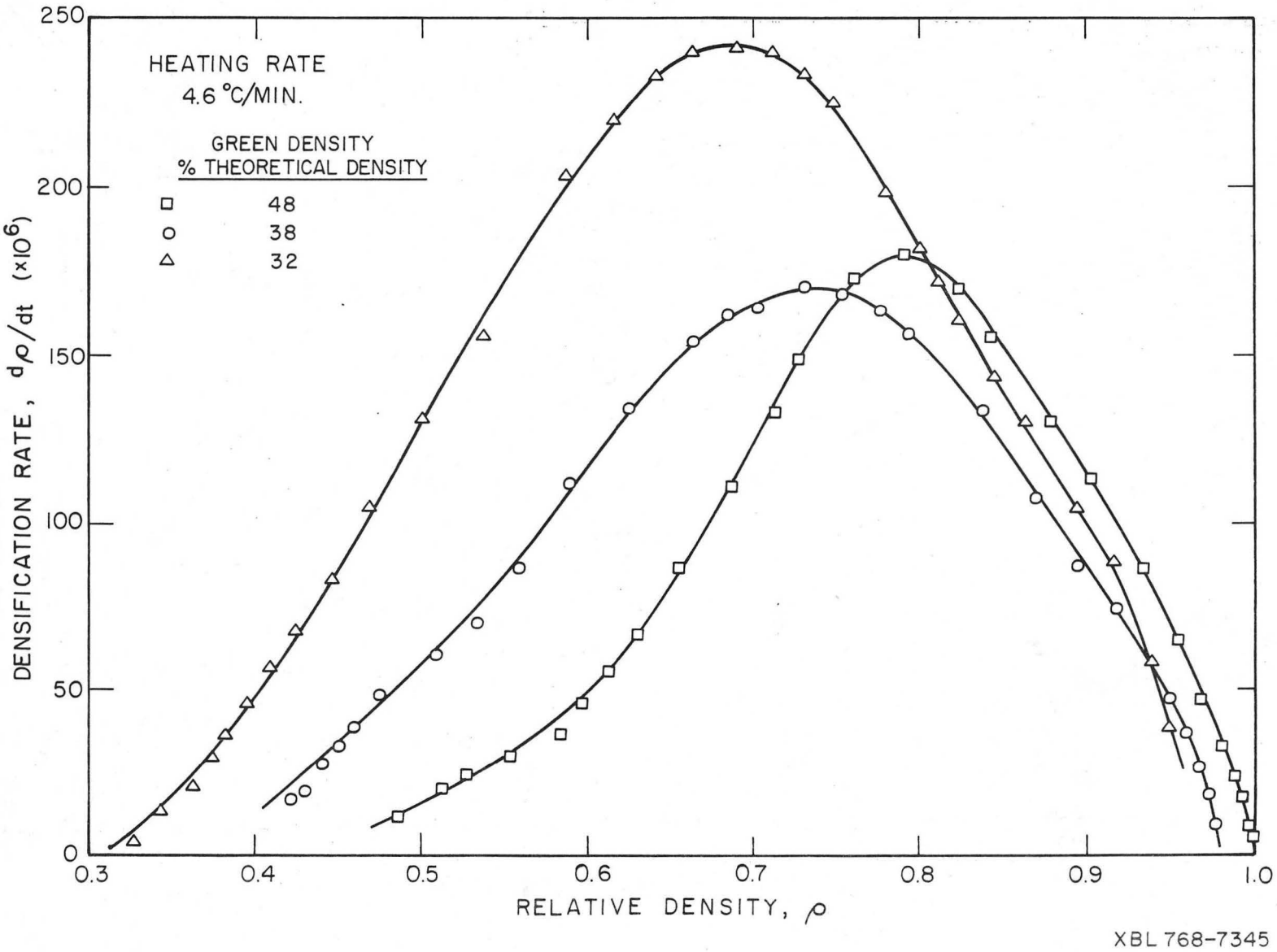
HEATING RATE
4.6 °C/MIN.
GREEN DENSITY
% THEORETICAL DENSITY
48
38
32
DENSIFICATION RATE, dρ/dt (×10⁶)
RELATIVE DENSITY, ρ
250
200
150
100
50
0
0.3
0.4
0.5
0.6
0.7
0.8
0.9
1.0
XBL 768-7345

Figure 8.

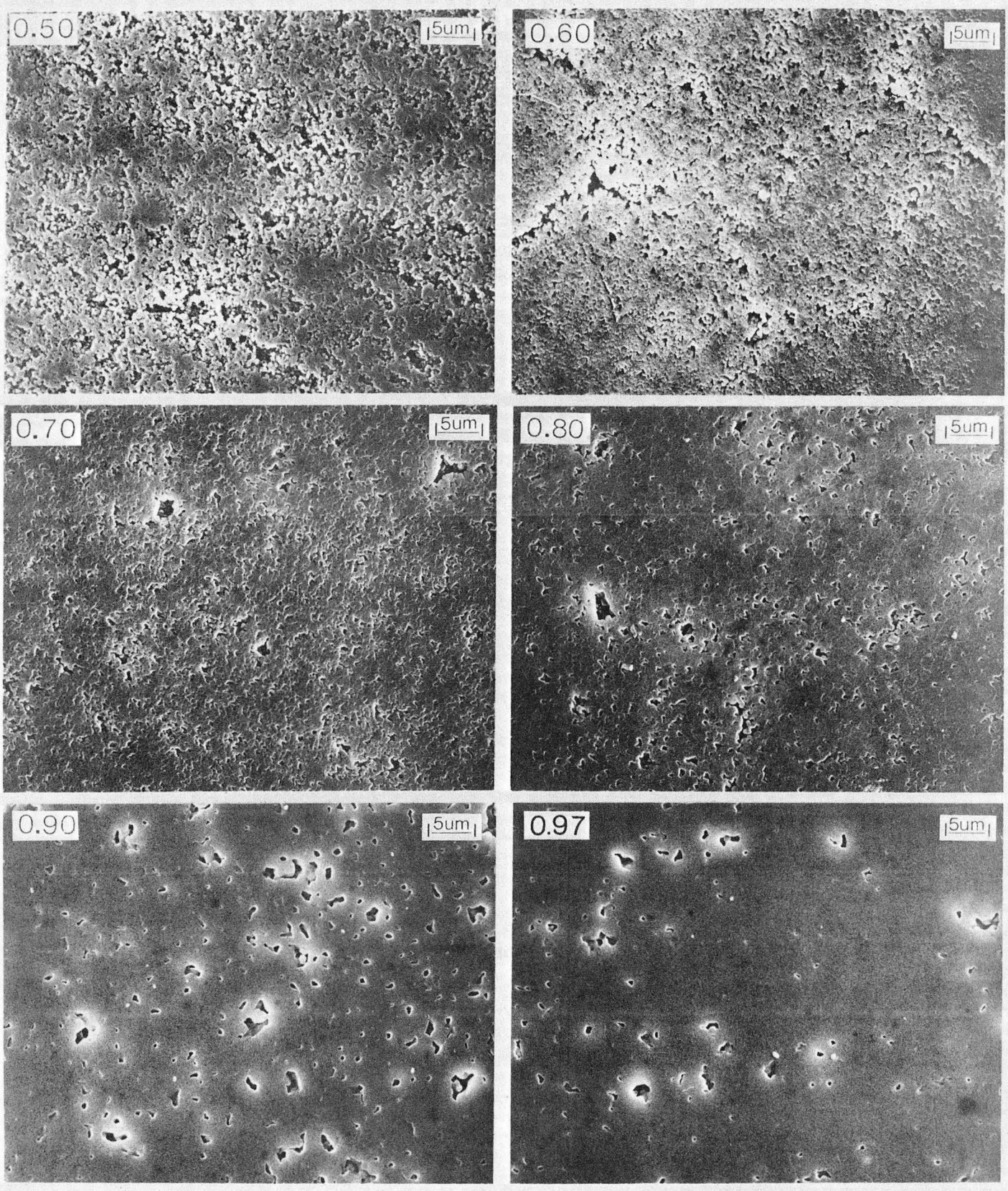

XBB768-7114

Figure 9.

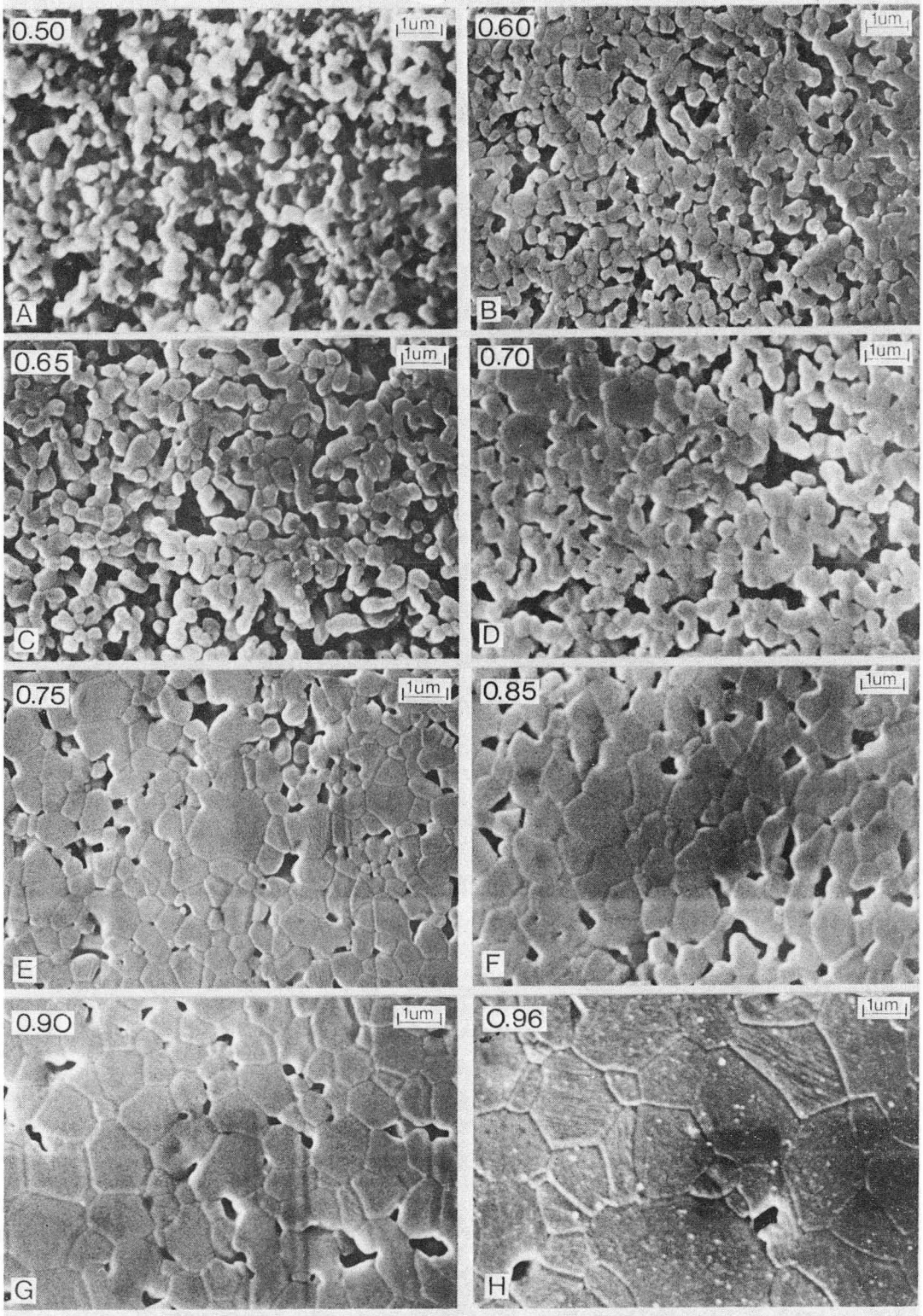

XBB768-7102

Figure 10.

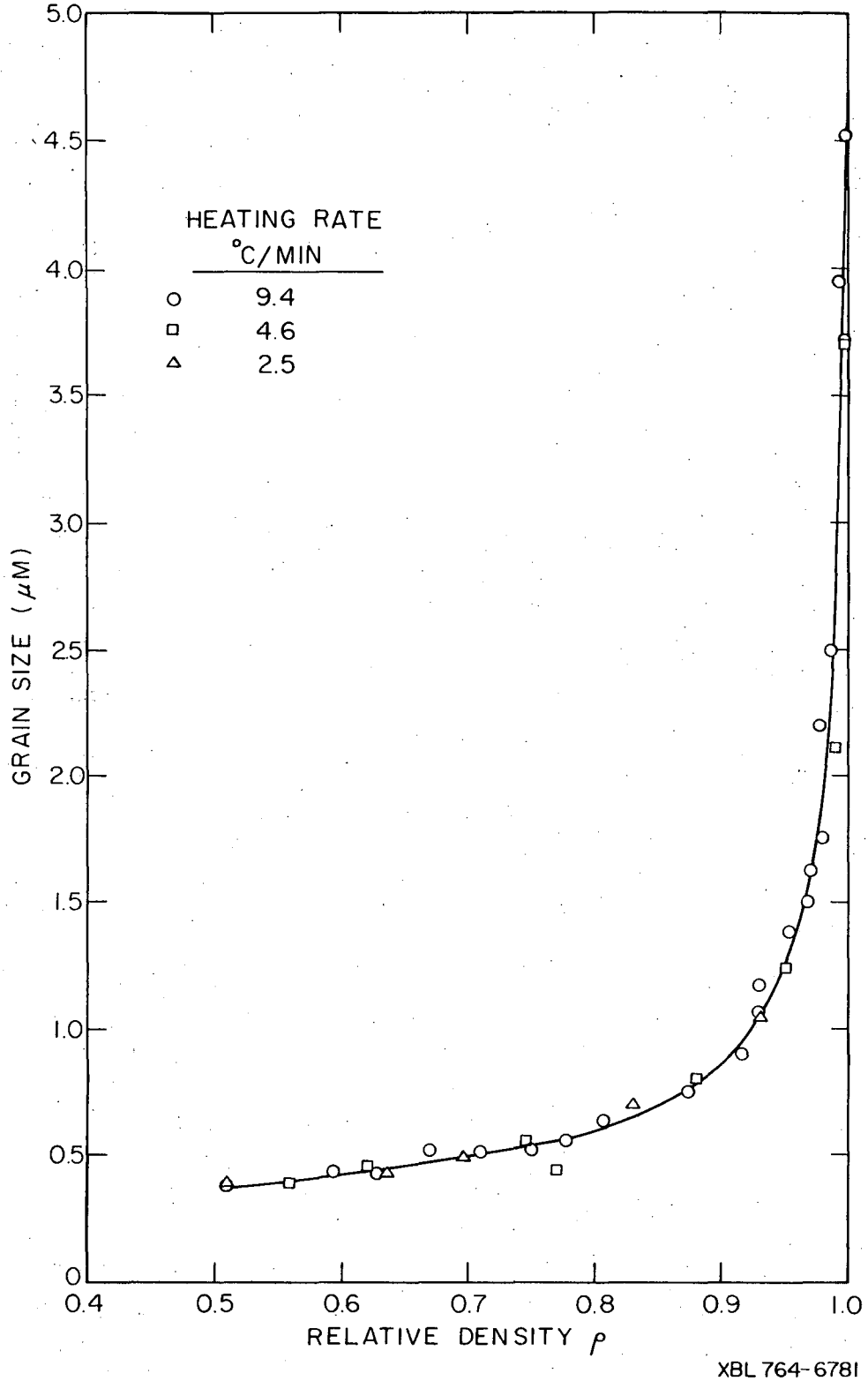
HEATING RATE
°C/MIN
9.4
4.6
2.5
GRAIN SIZE (μM)
RELATIVE DENSITY ρ
0
0.5
1.0
1.5
2.0
2.5
3.0
3.5
4.0
4.5
5.0
0.4
0.5
0.6
0.7
0.8
0.9
1.0
XBL 764-6781

Figure 11.

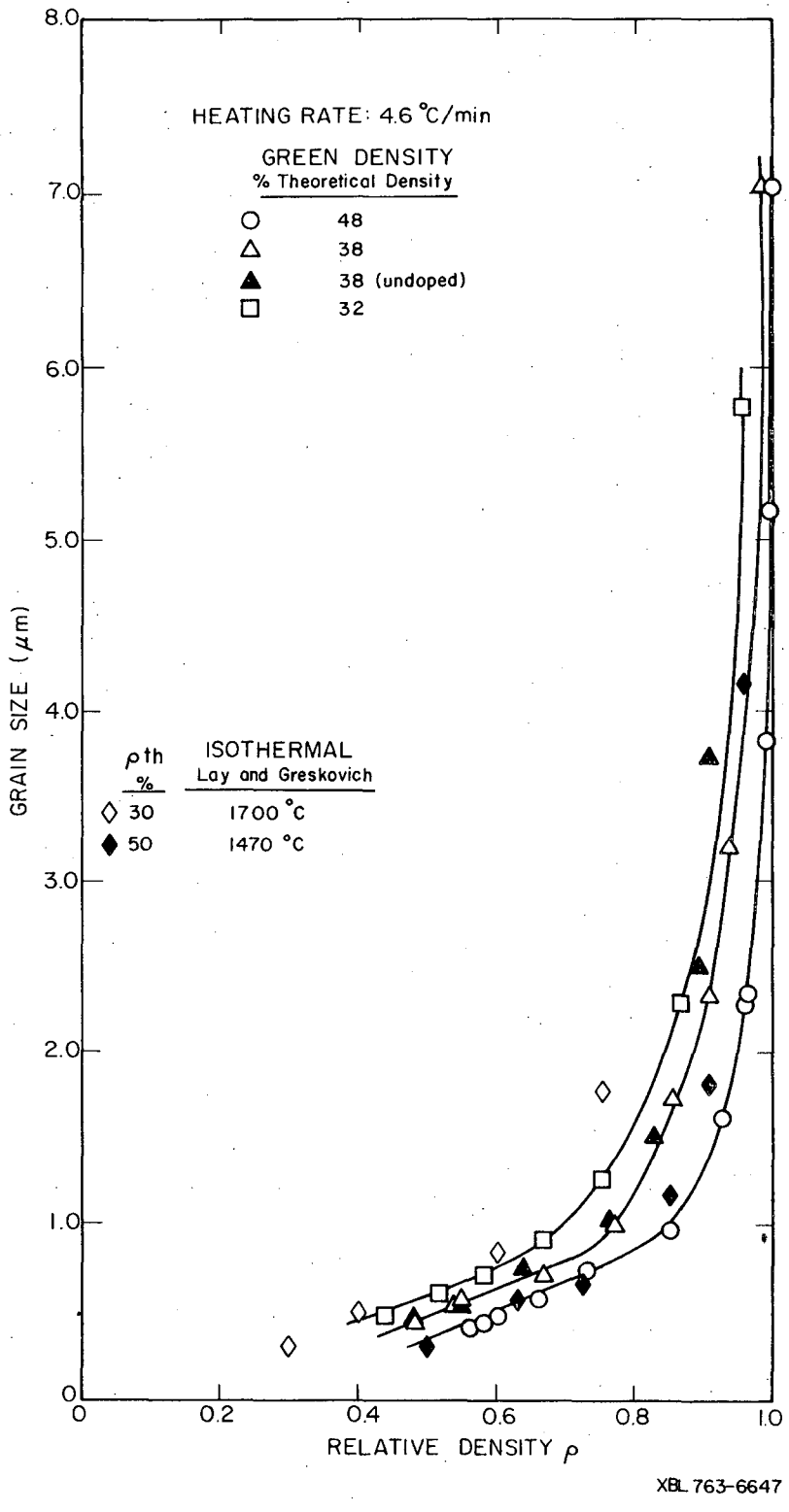
HEATING RATE: 4.6 °C/min
GREEN DENSITY
% Theoretical Density
48
38
38 (undoped)
32
ρth %
ISOTHERMAL
Lay and Greskovich
30
1700 °C
50
1470 °C
GRAIN SIZE (μm)
RELATIVE DENSITY ρ
0
1.0
2.0
3.0
4.0
5.0
6.0
7.0
8.0
0.2
0.4
0.6
0.8
1.0
XBL 763-6647

Figure 12.

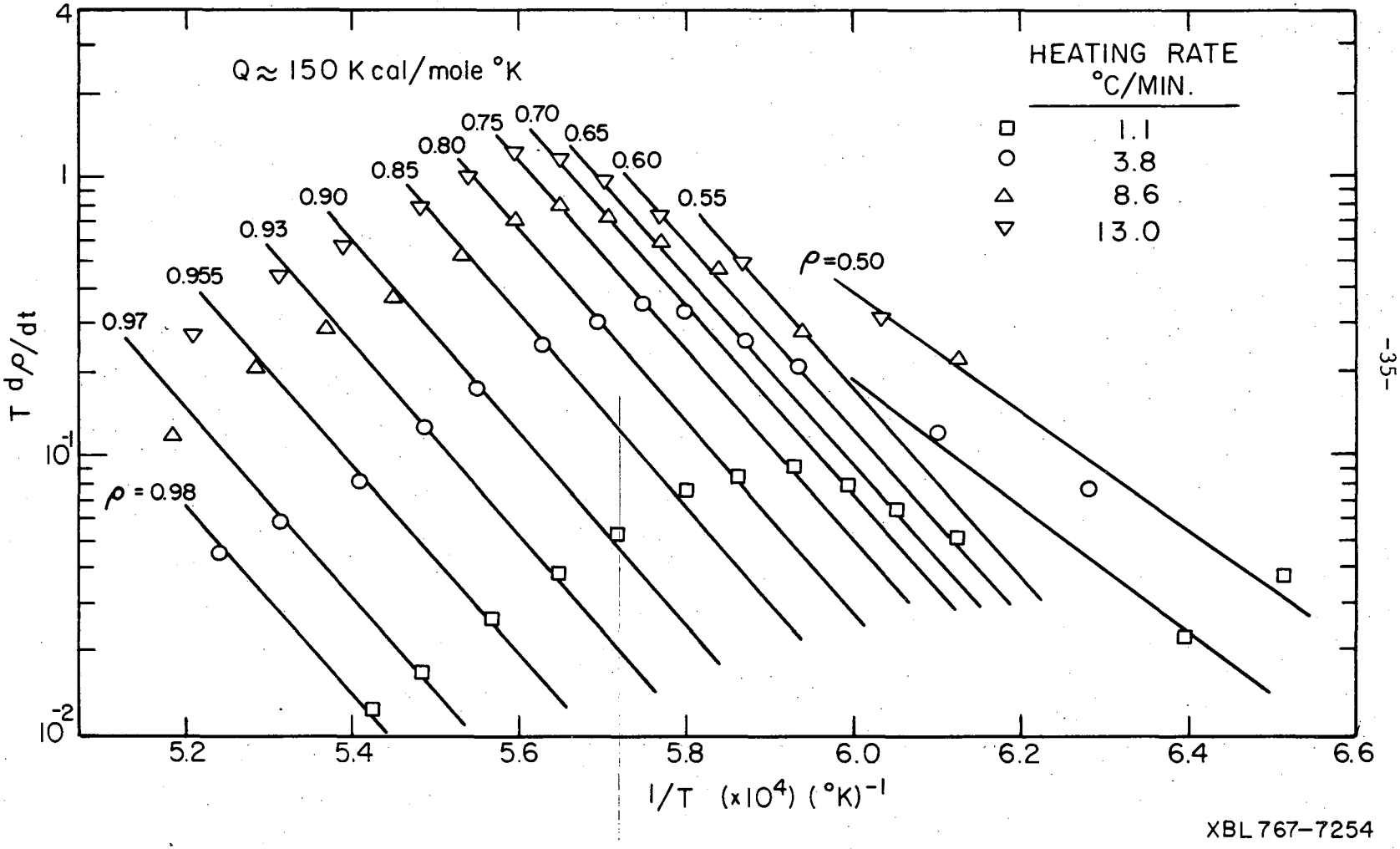

Figure 13.

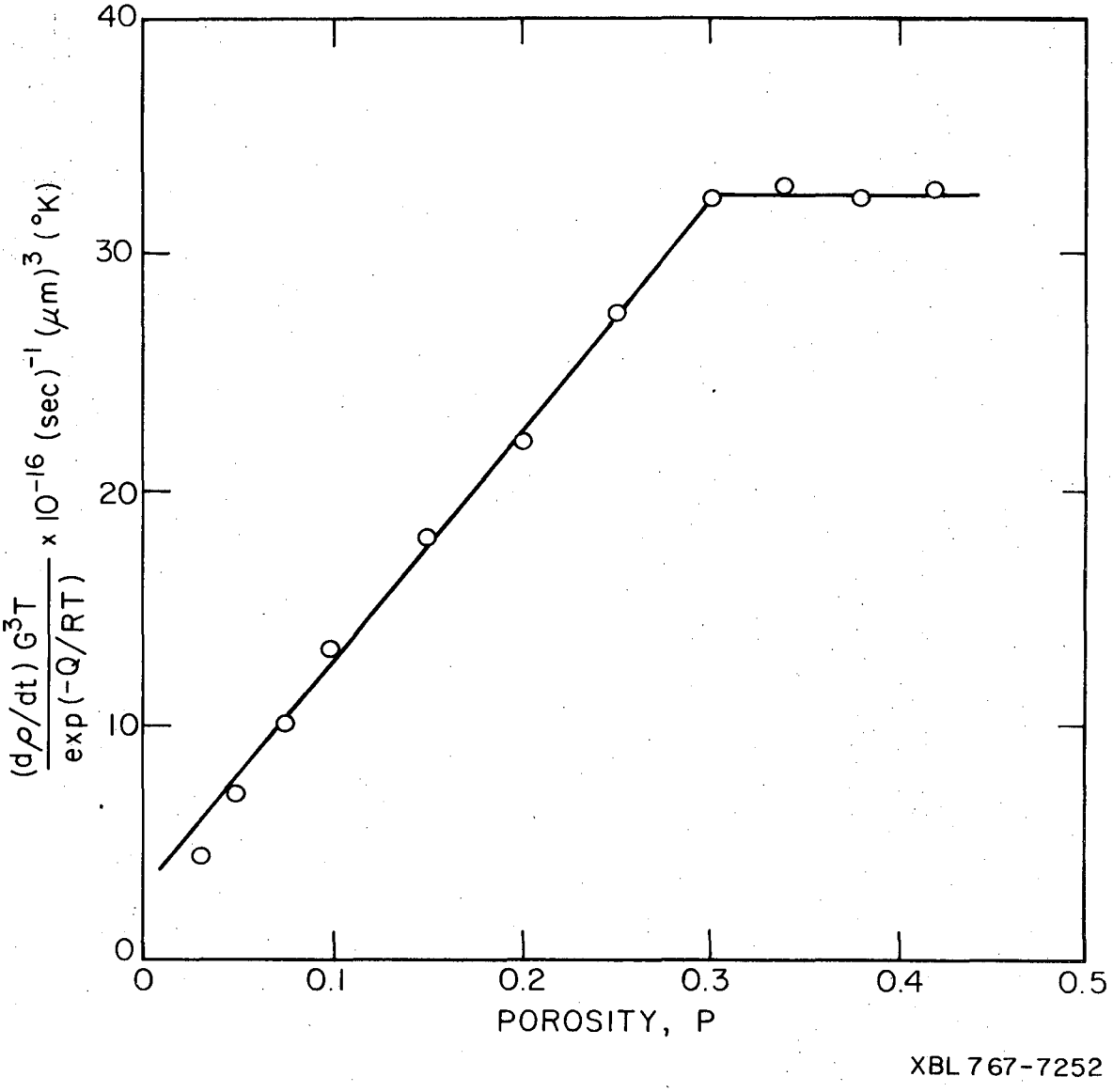
40
30
20
10
0
0
0.1
0.2
0.3
0.4
0.5
POROSITY, P
$\frac{(d\rho/dt)\,G^3T}{\exp(-Q/RT)} \times 10^{-16}\ (sec)^{-1}\ (\mu m)^3\ (°K)$
XBL 767-7252

Figure 14.

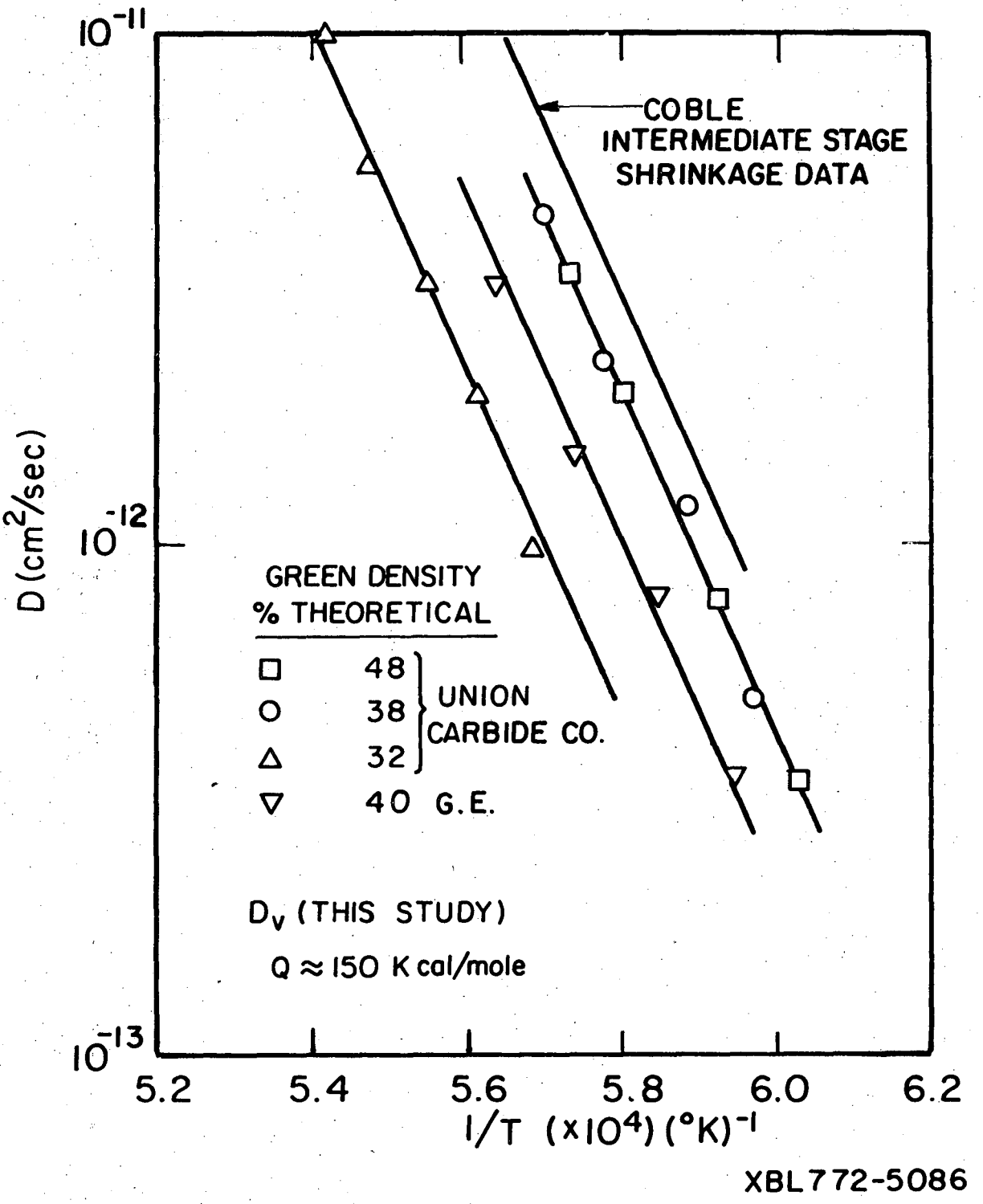

Figure 15.

This report was done with support from the United States Energy Research and Development Administration. Any conclusions or opinions expressed in this report represent solely those of the author(s) and not necessarily those of The Regents of the University of California, the Lawrence Berkeley Laboratory or the United States Energy Research and Development Administration.

TECHNICAL INFORMATION DIVISION
LAWRENCE BERKELEY LABORATORY
UNIVERSITY OF CALIFORNIA
BERKELEY, CALIFORNIA 94720